ACS OMEGA

Open Access

This article is licensed under CC-BY-NC-ND 4.0

http://pubs.acs.org/journal/acsodf

Article

Remarkably Enhanced Phosphate Sequestration from Waters by Biochar with High-Density Quaternary Ammonium Groups

Yan Li, Lili Dong, Xingyu Ren, Hao Liu, Chenjia Zhang, and Shunli Wan*

Cite This: *ACS Omega* 2024, 9, 20119−20128

Read Online

ACCESS | Metrics & More | Article Recommendations | Supporting Information

ABSTRACT: A new biochar (N-BC) was fabricated by incorporating high-density positively charged quaternary ammonium groups into the pristine biochar without any adsorption for phosphate. N-BC can highly efficiently remove phosphate with an optimal pH of 5.0, a maximum experimental adsorption capacity of 30 mg of P/g, and an adsorption equilibrium time of 180 min. The predicted pore diffusion coefficient D (the diffused surface area of the adsorbate for unit time) for phosphate adsorption by N-BC was 5.3×10^{-9} cm^2/s. N-BC can still capture phosphate in the copresence of anion Cl^- with a molar concentration 50 times that of phosphate. The exhausted N-BC was completely regenerated using a 10 wt % NaOH solution and further reused without any observable loss in adsorption capacity. Moreover, N-BC yielded ∼324 bed volumes (BV) of wastewater containing 1 mg P/L phosphate and 50 mg/L Cl^- before breakthrough occurring (<0.1 mg P/L in effluent) in a fixed-bed column operation system. The introduced quaternary ammonium groups covalently bound to biochar played a dominant role in phosphate sequestration by N-BC through forming the out-sphere complexation with phosphate. All results imply that it is of promising prospect for N-BC practical application for phosphate purification from waters. The present study provided a new strategy to expand the application of biochar, usually serving as an adsorbent for cationic pollutants, to the purification of anionic pollutants such as phosphate from waters.

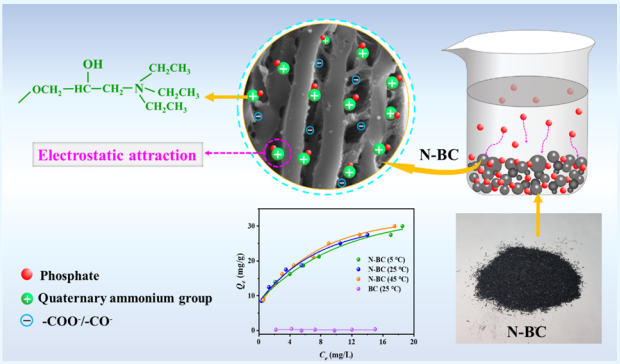

1. INTRODUCTION

Phosphorus, an indispensable nutrient for aquatic ecosystems, has been generally acknowledged as the chief culprit in undesirable eutrophication.[1−3] Meanwhile, it is also a scarce and nonrenewable resource.[4] As a result, the removal and recovery of phosphorus are always a widely concerned environmental focus. Phosphate is the dominant species of phosphorus in water, also the most easily assimilated by autotrophs.[5] Currently, numerous techniques including chemical precipitation,[6] adsorption,[7,8] and biological processes[9,10] have been developed for phosphate removal from waters. Among them, chemical precipitation and biological processes achieved wide field applications because of their convenient operation and relatively low cost.[11,12] However, with the ever-stringent emission standard of phosphorus (e.g., 0.5 mg of P/g for municipal drainage), these conventional techniques are difficult to be competent for the efficient removal of phosphate at such a low level. Moreover, a mass of byproduct sludge needs appropriate disposal, otherwise it easily generates secondary pollution.[12,13] In comparison, adsorption has brought about increasing attention to phosphate decontamination from waters because of the cleaner process and more suitable for sequestrating phosphate at low concentrations.[14] More attractively, it is considered that adsorption is an effective way to recycle phosphorus resources from the effluents.[15] Over the past decade, a variety of adsorbents had been exploited for phosphate retention, such as biomass,[16] metallic oxides,[7] biochar,[17] and polymers.[18,19]

Biochar, a carbon-rich porous solid with unique properties including great physicochemical stability, low cost, and wide availability as well as achieved carbon sequestration has enjoyed great popularity in various fields in virtue of its multiuse, e.g., adopted as capacitors, catalyst supports,[20−22] and adsorbents. It originated from the thermal decomposition of biomass, such as oak wood, rice husk, pine, corn straw, soybean straw, and peanut straw, in a reactor with little or no available air and at moderate temperatures (usually lower than 700 °C).[23] During pyrolysis, a considerable amount of oxygen-containing functional groups such as hydroxyl and carboxyl groups is generated.[24,25] These negative groups can form out-sphere complexation with numerous cations, making biochar an increasingly attractive adsorbent for decontamination of

Received: December 31, 2023
Revised: April 4, 2024
Accepted: April 18, 2024
Published: April 26, 2024

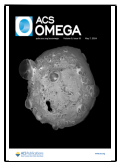

© 2024 The Authors. Published by American Chemical Society

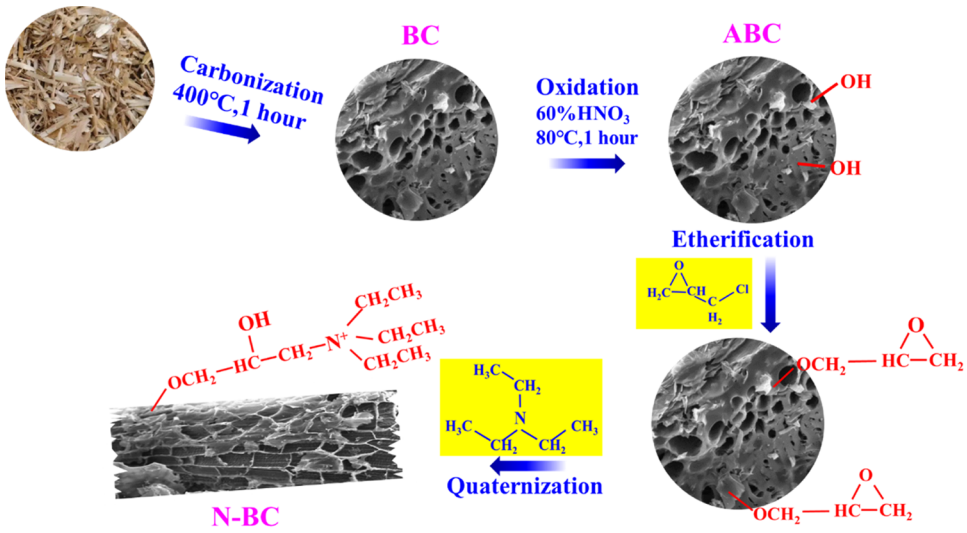

Figure 1. Schematic fabrication procedures of the as-obtained N-BC.

cationic pollutants (e.g., heavy metals) in the water treatment field.[26] In recent years, some attempts were made to expand the application of biochar as an adsorbent to the cleanup of anionic contaminates like phosphate, but outcomes were poor.[27] For example, peanut shell-based biochar only obtained a predicted adsorption capacity of 6.79 mg/g for phosphate;[28] however, maize straw and rice husk-based biochar had almost no adsorption for phosphate in waters.[29] The Coulomb repulsion resulting from the negative surface of biochar is the primary cause for the paralyzed adsorption of biochar to anionic contaminants. Therefore, it would be feasible to enormously boost the biochar adsorption toward anionic pollutants such as phosphate by changing the biochar surface to a positively charged one.

The introduction of amine groups such as the quaternary ammonium group is a conventional practice to enhance the surface electropositivity of materials.[30] For example, the surface of biomass (e.g., wheat straw and corn staw)[31−33] had been successfully changed to a positively charged one by grafting quaternary ammonium groups by means of the combined processes of oxidation, etherification, and quaternization in sequence. As a consequence, the modified biomass exhibited impressive adsorption toward phosphate in waters, as expected.[31,34] Therefore, it is considered that this strategy should also be competent for the preparation of positively charged biochar for phosphate adsorption.

The main objective of the current study is to prepare a positively charged biochar with high adsorption capacity and a stable regenerable property for phosphate removal from contaminated waters. The resultant adsorbent, a positively charged biochar (N-BC), was synthesized by processing the pristine biochar in accordance with the sequence of oxidation, etherification, and quaternization. The adsorption performance of phosphate on N-BC was examined as a function of the pH effect, the impact of coexisting substances, isotherm, and kinetics. Moreover, the adsorption mechanism was also uncovered with the help of Fourier transform infrared spectrometry (FTIR) and X-ray photoelectron spectroscopy (XPS) analysis. In addition, the practical application feasibility of N-BC for phosphate decontamination was further investigated by carrying out fixed-bed adsorption experiments by employing a challenging synthetic phosphate-polluted wastewater as a feeding solution.

2. MATERIALS AND METHODS

2.1. Materials. All chemicals were purchased from Aladdin Industrial Corporation except for humic acid (HA) that was provided by Aldrich-Sigma. These chemicals were analytical reagent grade (AR) or better and directly used without any pretreatment. A 1000 mg/L phosphate stock solution was obtained by dissolving KH_2PO_4 into ultrapure water with resistivity higher than 18.25 MΩ·cm. It was subjected to a stepwise dilution for further experimental uses. Corn stalk (CS) was used as the precursor for biochar and acquired from the farmland in Huangshan City, China. The compared adsorbent D201, a commercial phosphate adsorbent, was derived from Zhejiang Zheng Guang. Co., Ltd. D201 was covalently bound with abundant quaternary ammonium groups, i.e., $-N^+(CH_3)_3$, with a BET surface area of ∼10.5 m^2/g and an average pore diameter of 24.8 nm.

2.2. Synthesis of N-BC. Figure 1 illustrates the graphic route of the N-BC fabrication. As depicted, the preparation process can be divided into two procedures, i.e., the production of the pristine biochar (BC) and the following modification. In detail, the raw biochar was produced from the pyrolysis of CS in the atmosphere of Ar according to the conventional technique of biochar preparation[23] with a maximum holding temperature of 400 °C and a heating rate of 15 °C/min. Subsequently, the as-obtained BC of 1.0 g was immersed into the HNO_3 solution of 60% in volume ratio, followed by nonstop stirring for 1 h at 80 °C. The oxidization of HNO_3 can introduce abundant hydroxyl groups covalently bound to biochar. The solids were then fetched out and washed until around neutral pH and immediately swollen for 4 h in N,N-dimethylformamide (DMF) solution. After that, a predesigned amount of epichlorohydrin was dropwise injected into the solution along with continuous agitation for 2 h at 80 °C, and then a small amount of ethanediamine was instilled, accompanied by constant stirring for 1 h. During this process, the added epichlorohydrin reacted with hydroxyl groups to form epoxy groups covalently bound to the biochar through etherification. Afterward, triethylamine was dripped into the above solution, followed by continuous stirring for another 2 h.

https://doi.org/10.1021/acsomega.3c10526
ACS Omega 2024, 9, 20119−20128

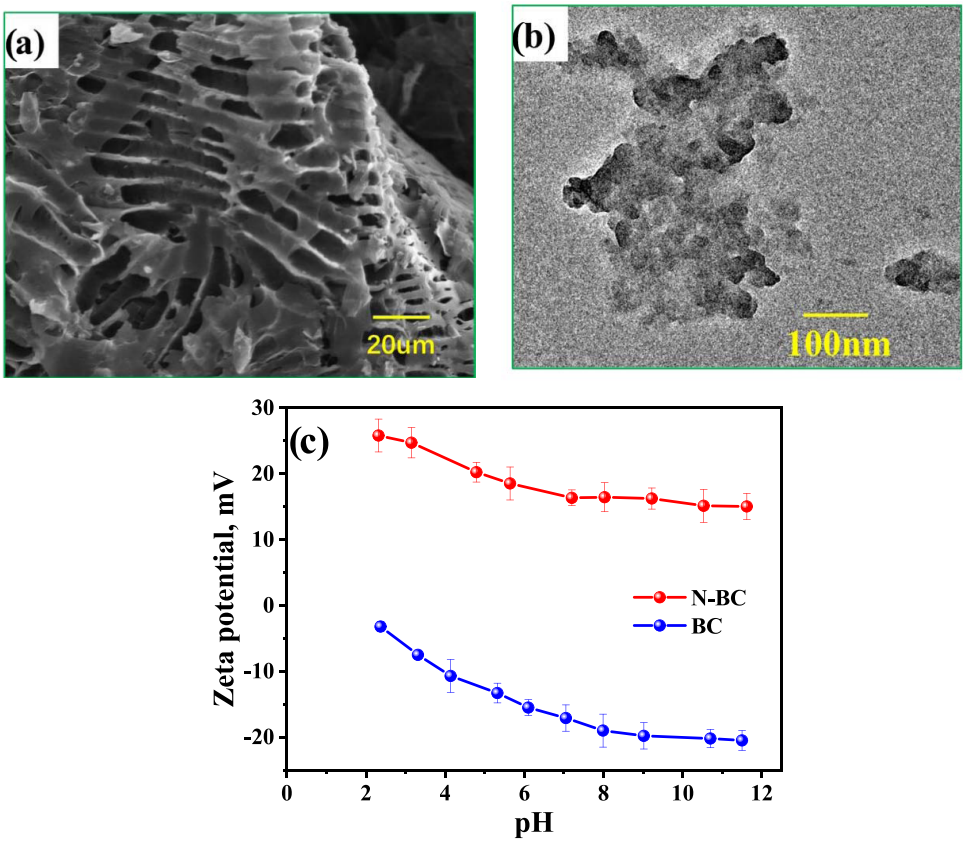

Figure 2. (a) SEM image of N-BC, (b) TEM image of N-BC, and (c) the ζ potential analysis of N-BC and the pristine BC.

The added triethylamine reacted with epoxy groups to form quaternary ammonium groups that were covalently bound to biochar through quaternization. After all of the procedures, the biochar was filtered out from the solution and subjected to alternate flushing by HCl, NaOH, and ethanol solution. The solids were further desiccated at 60 °C until they reached the constant mass, and then, N-BC with high-density quaternary ammonium groups was obtained. The resultant N-BC was crushed into particles of 0.15−0.25 mm prior to use.

2.3. Batch Adsorption Experiments. On the frequently used bottle-point method, the batch experiments were carried out in 100 mL Erlenmeyer flasks. In brief, 0.01 g of N-BC or D201 was immersed into Erlenmeyer flasks containing 50 mL of solution of phosphate at a preset level. The solution pHs were adjusted to desired values using HCl or NaOH solutions of different concentrations. The impact of coexisting substances was investigated by employing Na_2SO_4, $NaNO_3$, Na_2CO_3, NaCl, and HA as interfering substances. The prepared flasks were fastened in a thermostatic orbit incubator equipped with a gas bath and oscillated for 24 h at 180 rpm and 298 K. The time of 24 h was proven to be sufficient for achieving the adsorption equilibrium based on the preliminary kinetic experiments. In the kinetic experiment, 0.5 mL of the supernatant was taken out at predetermined time intervals to detect the concentration of phosphate. According to the principle of mass balance, the adsorption capacity as well as the removal rate of the targeted pollutant was acquired.

2.4. Fixed-Bed Column Tests. The device of the fixed-bed column is illustrated in Figure S1. In fixed-bed column experiments, a 5 mL aliquot of wet N-BC or D201 was first packed within the glass column (12 mm in diameter and 130 mm in length) equipped with a water bath to maintain the desired temperature. Then, the feeding solution passed through the bed of the adsorbent from top to bottom with a constant flow rate controlled by a speed-adjustable Lange-580 pump (Baoding, China). The effluents were gathered using an automatic partial collector, and phosphate content was analyzed at desired intervals of bed volumes (BV). After the breakthrough, the exhausted adsorbent was subjected to in situ regeneration by the 10 wt % NaOH solution. The components of phosphate-containing wastewater and regenerant, as well as the operation parameters, were presented in the caption of the related figure.

2.5. Analyses and Characterization. On the basis of the molybdenum blue spectrophotometric method, the phosphate level was detected using the UV/vis spectrometer (T6, PGENERAL, China). The specific surface area and the average pore size of N-BC were obtained by employing the Micromeritics ASAP2020 instrument. The morphology and structure of N-BC were observed through a scanning electron microscope (SEM, S-3400N, Japan) and a transmission electron microscope (TEM, Tecnai G2 F30 S-Twin, Holland) equipped with a field emission gun at 200 kV. ζ potentials of N-BC and the pristine biochar were measured by employing a Malvern Zetasizer Nano ZS90. FTIR spectra of N-BC before and after phosphate adsorption were collected using Fourier transform infrared spectroscopy (Nicolet 6700) in the wavenumber range of 400−4000 cm^{-1}. The interaction of N-BC and phosphate was probed with the aid of X-ray photoelectron spectroscopy (XPS, Kratos AXIS Ultra DLD, Japan) according to well-established methods with Al Kα irradiation as the excitation source. The C 1s peak located at

https://doi.org/10.1021/acsomega.3c10526
ACS Omega 2024, 9, 20119−20128

284.8 eV was employed to adjust the as-acquired binding energies, and the profile-fitting program XPSPEAK4.1 (Raymund W.M. Kwok, Hong Kong) was used to process the collected data.

3. RESULTS AND DISCUSSION

3.1. Characterization of N-BC. The resultant material N-BC has a similar appearance including shape and color as the pristine BC, according to Figure S2. From SEM and TEM images of N-BC in Figure 2a,b, it can be observed that there are abundant microsized holes in the skeleton of N-BC, and the surface of N-BC is uneven. After modification of BC, there is a slight increase in the average pore size and specific surface area, i.e., 17.6 nm and 6.2 m^2/g for N-BC and 16.3 nm and 5.8 m^2/g for BC, respectively. Moreover, the pores of N-BC are mainly micropores and mesopores, according to the pore distribution curve in Figure S3. The ζ potential profiles of BC and N-BC are compared in Figure 2c. As illustrated, the consistently negative ζ potential of the pristine BC in the tested pH range of 2.0−12.0 indicates that its surface is negatively charged, brought about by the self-attached oxygen-containing groups like hydroxyl and carboxyl groups. Comparatively, the ζ potential values of the as-obtained N-BC (from 25.3 to 15.8 mV) are always greater than zero, suggesting a highly positively charged surface. It can preliminarily be seen that the quaternary ammonium groups were successfully introduced into biochar as expected. From the compared FTIR spectra of BC and N-BC in Figure S4, it is clear that a sharp peak located at the wavenumber of ∼1384 cm^{-1} occurs, assigned to the vibration of the quaternary ammonium groups (i.e., the presence of quaternary ammonium-type nitrogen).[32] It further confirms the successful incorporation of the desired quaternary ammonium functional groups in N-BC.

3.2. Effect of Solution pH on Phosphate Adsorption. The adsorption process usually changes greatly with varying solution pH values on account of the transformations of the present species of the adsorbate and the chemical properties of the adsorbent. Given this, the effect of solution pH on phosphate sequestration by N-BC was examined, and the results are shown in Figure 3. As depicted, in the listed pH range of 2.0−12.5, phosphate removal onto N-BC was obviously associated with solution pH, and the optimal pH was around 5.0. Specifically, at the right of optimal pH, phosphate removal continuously decreased with the increased solution pH, and the adsorption capacity decreased to near 1.5 mg/g at pH 12.5. It should be put down to the ever-decreasing electropositivity of N-BC with the increased pH (favored by Figure 2c). That is, the interaction between N-BC and the negative phosphate constantly declined. Unexpectedly, at the left of optimal pH, phosphate adsorption also dropped with the pH decreasing, which is supposed to be ascribed to the transformation of the dominating phosphorus species from negative $H_2PO_4^-$ to neutral H_3PO_4 (Figure S5). In other words, with pH declining, the ζ potential of N-BC increases and the electrostatic attraction of N-BC to the negative phosphate ion also strengthens, but more and more negative $H_2PO_4^-$ transforms into neutral H_3PO_4, which cannot be adsorbed on N-BC by electrostatic attraction. On the basis of the aforementioned results, it is speculated that N-BC can be efficiently used for the cleanup of phosphate-containing wastewater of pH 3.0−9.0; moreover, the adsorbed phosphate on N-BC can be effectively eluted and recycled using alkali solution.

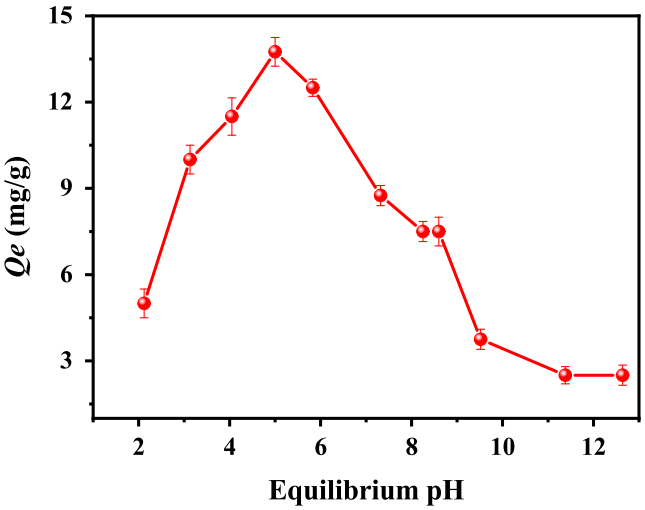

Figure 3. Effect of pH on phosphate adsorption by N-BC. Conditions: C_0 (phosphate) = 5 mg P/L, sorbent dose = 0.2 g/L, and temperature = 298 K.

3.3. Influence of the Coexisting Substances on Phosphate Adsorption. Naturally occurring anions such as Cl^-, NO_3^-, SO_4^{2-}, and CO_3^{2-} usually generate great interference in the adsorption of phosphate. Herein, the influence of these anions on phosphate adsorption by N-BC was evaluated with D201 as a reference, and the results are presented in Figure 4a. As shown, when coexisting anions in solution were steadily increased, phosphate removal on both N-BC and D201 was impacted to varying degrees. For instance, increasing the molar concentrations of Cl^-, NO_3^-, SO_4^{2-}, and CO_3^{2-} from 0 to 50-fold of phosphate (0.06 mmol P/L) resulted in drops of ∼72, 84, 100, and 100% in phosphate adsorption capacities on N-BC, respectively. In an identical dosage of D201 (weight) as N-BC, the drops for D201 were ∼85, 100, 100, and 100%, respectively. Though phosphate adsorption onto N-BC suffered a great shock in the presence of ultrahigh levels of Cl^-, NO_3^-, and especially CO_3^{2-} and SO_4^{2-}, it was still comparable to or even superior to that of D201, a well-accepted prominent adsorbent for phosphate capture from waters. This suggests that the interaction of phosphate and N-BC was similar to that for phosphate and D201, that is, the nonspecific out-sphere complexation (i.e., Coulomb attraction). The underlying mechanism was probed with the aid of FTIR and XPS analysis and is further expounded in the subsequent section. The greater influence of CO_3^{2-} and SO_4^{2-} over Cl^- and NO_3^- on phosphate adsorption by the two adsorbents was attributed to their higher valence, that is, the greater Coulomb attraction with N-BC. Dissolved organic matter (DOM) in waters is also a great challenge for phosphate removal through the adsorption technique. Thus, the impact of humic acid (HA), a representative DOM, on phosphate adsorption by N-BC and D201 was investigated. The results in Figure 4b show that the introduced HA nearly paralyzed phosphate adsorption on the two adsorbents, in line with our expectations. Visibly, if the highly efficient application of N-BC for cleaning the real phosphate-polluted wastewater including NOM and anions of high valence is to be achieved, some specific binding sites for

https://doi.org/10.1021/acsomega.3c10526
ACS Omega 2024, 9, 20119−20128

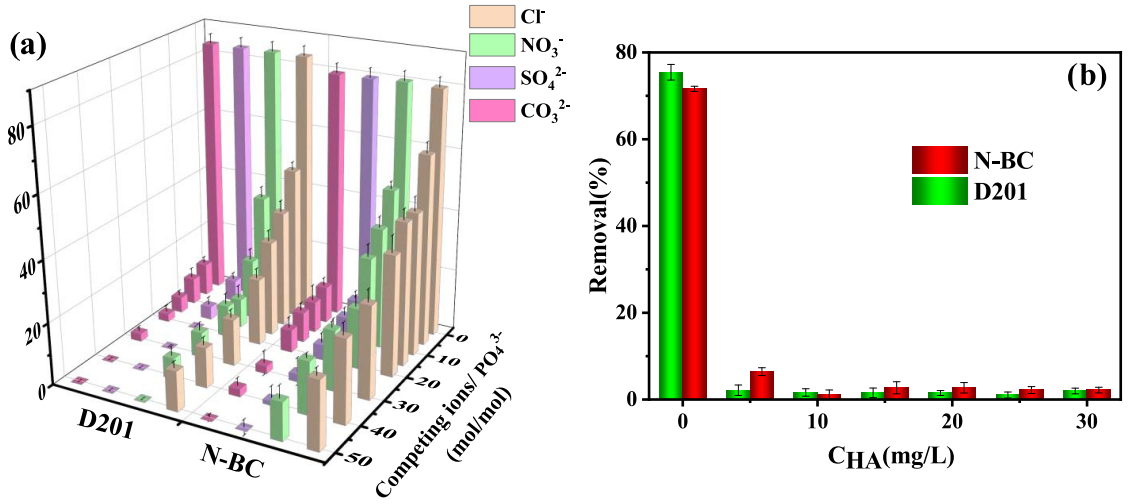

Figure 4. (a) Comparison of the impact of Cl^-, NO_3^-, SO_4^{2-}, and CO_3^{2-} at different levels on phosphate adsorption by N-BC and D201, and (b) the effect of HA on phosphate uptake by N-BC and D201. Conditions: C_0 (phosphate) = 2 mg P/L, sorbent dose = 0.2 g/L, pH = 4.5 ± 0.5, and temperature = 298 K.

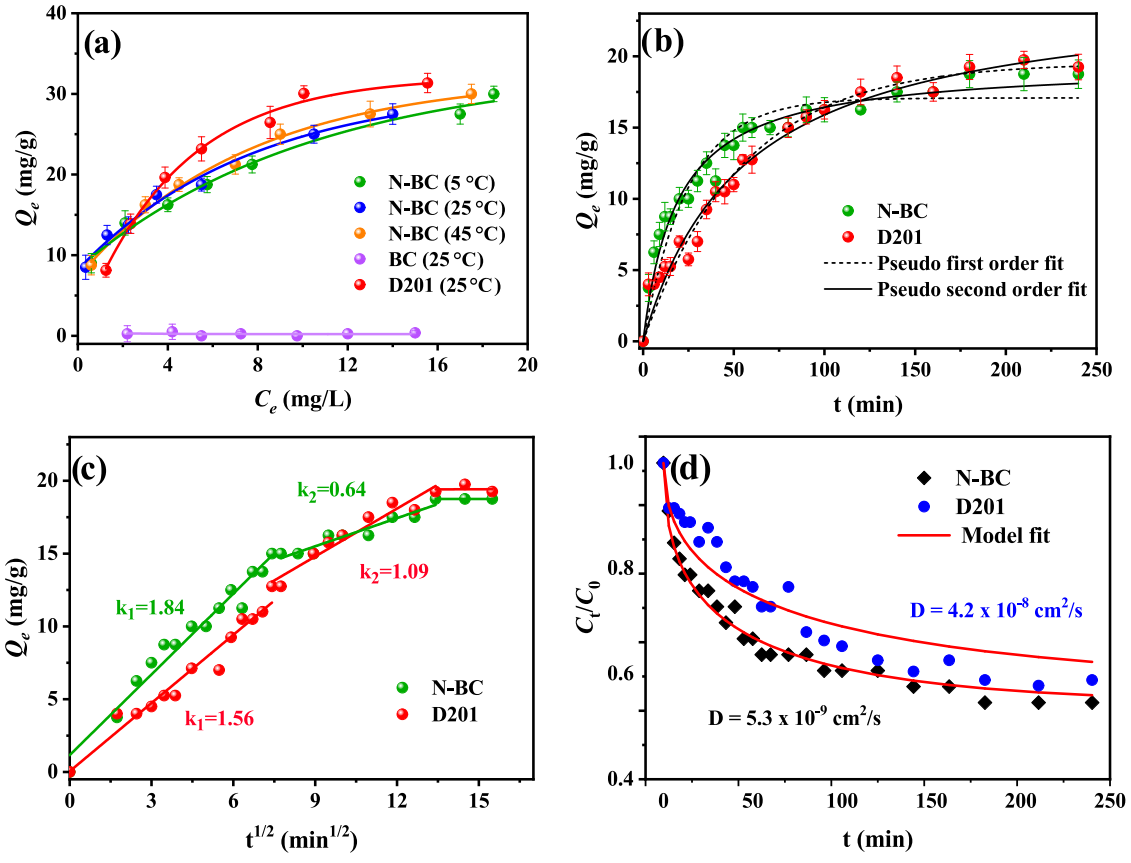

Figure 5. (a) Adsorption isotherms of phosphate onto N-BC (at 5, 25, 45 °C), BC, and D201 (at 25 °C), (b) the fitting of phosphate adsorption kinetics onto N-BC and D201 by pseudo-first- and pseudo-second-order models, (c) the fitting of phosphate adsorption kinetics onto N-BC and D201 by the intraparticle diffusion model, and (d) the fitting of phosphate adsorption kinetics onto N-BC and D201 by the model based on Fick's law. Conditions: C_0 (phosphate) for (b, c, d) = 8.5 mg P/L, sorbent dose = 0.2 g/L, pH = 4.5 ± 0.5, and temperature = 298 K.

phosphate need to be introduced into N-BC, such as impregnating metallic oxides.

3.4. Effect of Temperature on Phosphate Adsorption and Adsorption Kinetics. Figure 5a depicts the effect of temperature on phosphate retention by N-BC, with D201 and the pristine BC as a reference. It can be found that phosphate adsorption by N-BC was generally temperature-dependent, and increasing temperature from 5 to 45 °C was generally favorable for phosphate sequestration. The maximum experimental adsorption capacity of phosphate per gram of N-BC at 25 °C was ~30 mg of P, slightly lower than that of per gram of D201 (31.35 mg of P) but apparently greater than that of other biochar-based adsorbents (Table S1). It was expected that the pristine BC had no observable adsorption toward phosphate

https://doi.org/10.1021/acsomega.3c10526
ACS Omega 2024, 9, 20119−20128

due to the electrostatic repulsion of the negatively charged oxygen-containing groups covalently bound to BC toward the anionic phosphate.

The adsorption kinetics of phosphate by N-BC was also examined with D201 serving as a contrast, and the results are presented in Figure 5b. As shown, phosphate adsorption by both N-BC and D201 (identical weight in solution) was relatively rapid and approached equilibrium at approximately 180 min. Two classic kinetic models, i.e., pseudo-first- and pseudo-second-order models,[35,36] were first provided to predict the kinetics data.

$$\ln(q_e - q_t) = \ln q_e - \frac{k_1}{2.303}t \tag{1}$$

$$q_t = \frac{k_2 q_e^{\,2} t}{t k_2 q_e + 1} \tag{2}$$

Here, q_e and q_t (mg/g) represent the adsorption capacities of the adsorbate at equilibrium and at time t (min), respectively. k_1 and k_2 (mg/g·min$^{-1/2}$) denote the first- and second-order adsorption rate constants, respectively. From Figure 5b, it can be seen that phosphate adsorption kinetics onto both N-BC and D201 is in good agreement with the pseudo-second-order model of the related coefficient higher than 97%. According to the fitting results, the phosphate adsorption process seemingly consisted of two stages, that is, the rapid adsorption phase approximately from 0 to 60 min and the slow one from about 60 to 180 min. This is a typical intraparticle diffusion pathway. Consequently, the phosphate adsorption kinetics was also described by the intraparticle diffusion (IPD) model,[37] and the fitting profiles are presented in Figure 5c.

$$q_t = k_1 t^{1/2} + C \tag{3}$$

Herein, q_t (mg/g) is the amount of adsorbed phosphate at time t (min), k_1 is the diffusion rate (mg/g·min$^{-1/2}$), and C denotes the intercept. As shown, the IPD model excellently predicted the adsorption kinetics of phosphate; moreover, it precisely distinguished the aforementioned two stages. These two steps should represent the directed migration of phosphate from the solution to the outer surface of N-BC or D201 and the following diffusion to the binding sites across the pore channel, respectively. Obviously, the second phase diffusion, i.e., the pore diffusion, was the rate-controlling step of phosphate adsorption by N-BC and D201. The higher diffusion of D201 than that of N-BC (1.09 vs 0.64 mg/g·min$^{-1/2}$) in the second stage was caused by its greater pore diameter of 24.8 nm compared to that of N-BC (13.4 nm).

As for the IPD-controlled adsorption process, another kinetic model based on Fick's second law[38] can usually be used to quantify the effective coefficient of pore diffusion (D). Herein, phosphate adsorption kinetics was further predicted using this model by assuming that N-BC was a perfect sphere.

$$\frac{\partial q}{\partial t} = D\left(\frac{\partial^2 q}{\partial r^2} + \frac{2}{r}\frac{\partial q}{\partial r}\right) \tag{4}$$

Here, q (mg/g) represents the adsorbed amount of phosphate at time t (min), and r denotes the radial coordinate. In the present kinetics test, the solutions for the above equation at the initial and boundary conditions are shown as follows

$$q(0) = 0(0 \le r \le a) \tag{5}$$

$$\frac{\partial_q}{\partial_r} = 0(r = 0) \tag{6}$$

$$\frac{\partial_q}{\partial_r}\frac{3DM}{\alpha} = -V\frac{\partial_c}{\partial_t}(r = a) \tag{7}$$

wherein M (g) and V (L) denote the mass of the adsorbent and the volume of the solution, respectively. a (mm) denotes the average size of the adsorbent, which is 0.2 and 0.75 mm for N-BC and D201, respectively, obtained from the statistical analysis of their typical optical microscope photographs. At adsorption equilibrium, the solution for eq 4 is as follows.

$$F = \frac{q(t)}{q_e} = 1 - \sum_{n=1}^{\infty}\frac{6\alpha(\alpha+1)\exp(-Dq_n^{\,2}t/a^2)}{9 + 9\alpha + q_n^{\,2}\alpha^2} \tag{8}$$

In which q_e (mg/g) is the adsorption capacity of phosphate at equilibrium, and α is a variable denoting the ultimate fractional capacity of phosphate, which can be calculated based on the following equation.

$$\frac{Mq_e}{V_0 C_0} = \frac{1}{\alpha + 1} \tag{9}$$

In which V_0 (L) and C_0 (mg/L) represent the initial volume of the solution and phosphate concentration, respectively. q_n is a predesigned variable gained by the following equation.

$$\tan q_n = \frac{3q_n}{3 + \alpha q_n^{\,2}} \tag{10}$$

The solution for the above equation can be acquired according to the bisection method in the given intervals.

The amount of phosphate in the solution/adsorbent at different times can be easily gained on the basis of the mass-balance principle. Through constantly changing D values, the optimal fitting results for phosphate adsorption kinetics on N-BC and D201 were generated (Figure 5d). The predicted D values of N-BC and D201 are 5.3×10^{-9} and 4.2×10^{-8} cm^2/s, respectively. Compared to N-BC, D201 possessed a greater D value owing to its higher average pore size, which is consistent with the aforementioned result. For comparison, phosphate diffusivity in aqueous solution (D_e) was also calculated based on the Stock−Einstein equation as follows.

$$D_e = \frac{K_B T}{6\pi\mu R_0} \tag{11}$$

In which k_B (J/K) corresponds to the Boltzmann constant, 1.38×10^{-23} J/K, μ (N·s/m^2) is the water viscosity, 8.9×10^{-4} N·s/m^2 at 25 °C, R_0 (nm) denotes the ion radius of phosphate, 0.2 nm, and T (K) represents the temperature in Kelvin, 298 K. After necessary calculation, the D_e value of phosphate was determined to be 1.23×10^{-5} cm^2/s, much higher than the D values of its diffusion in the pore region of N-BC and D201. This is in accordance with the above-mentioned IPD fitting results; that is, phosphate diffusion in solution is much quicker compared to that in pores of adsorbents. It should result from the abundant micro- and mesopores inside N-BC or D201 impeding the diffusion of phosphate because of space confinement.

3.5. Fixed-Bed Column Adsorption Experiment. Fixed-bed column adsorption experiments are appropriate to investigate the application feasibility of the adsorbent with

https://doi.org/10.1021/acsomega.3c10526
ACS Omega 2024, 9, 20119−20128

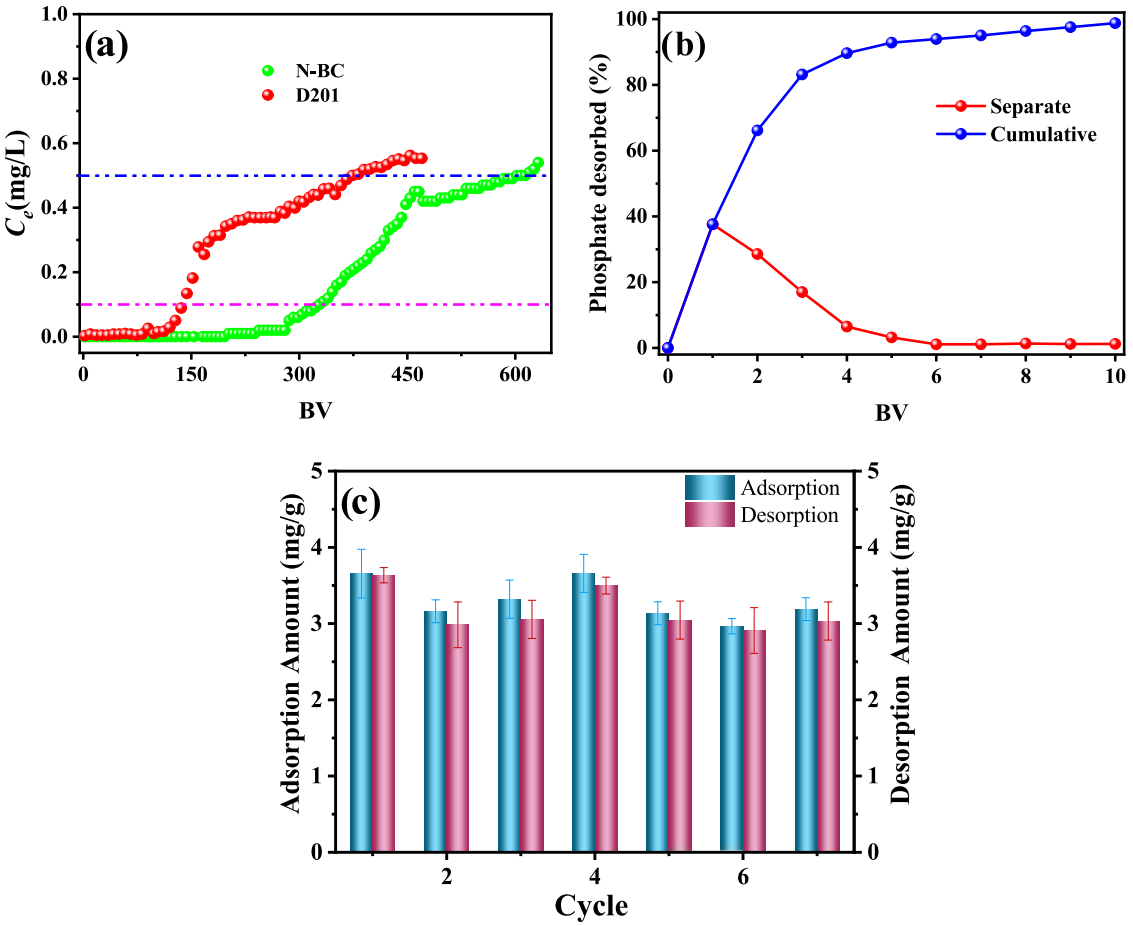

Figure 6. Breakthrough profiles of the fixed-bed packing N-BC and D201 with the synthetic phosphate-polluted wastewater as feeding solution, (b) the regeneration curves of the exhausted N-BC, and (c) the adsorption−desorption cycles of the resultant N-BC. Conditions for (a): the SLV and EBCT are 0.44 m/h and 31 min, respectively, and temperature = 298 K. The main composition of feeding solution: C_0 (phosphate) = 1.0 mg P/L, C_0 (Cl^-) = 50 mg/L, and pH = 6.0 ± 0.2. Conditions for (b): the SLV and EBCT are 0.04 m/h and 313 min, respectively, and temperature = 298 K. The main composition of the regenerant: 10% NaOH. Conditions for (c): C_0 (phosphate) = 8 mg P/L, sorbent dose = 1.0 g/L, pH for adsorption = 6.0 ± 0.2, and temperature = 298 K.

good hydraulic characteristics in a real scenario. As a consequence, the fixed-bed column tests of N-BC and the contrast D201 for decontaminating the phosphate-containing wastewater including the coexisting substances were operated, and the breakthrough curves are presented in Figure 6a. Of note, the added wet volume of N-BC and D201 in two columns is identical, i.e., 5 mL. As shown, in the presence of only Cl^- in influent, the N-BC column can generate ∼598 BV effluents of the phosphate level lower than 0.5 mg P/L, i.e., the breakthrough point, whereas that of D201 was only ∼374 BV. When the breakthrough point was set to 0.1 mg P/L, the effective treatable volumes of N-BC and D201 columns were ∼324 and 140 BV, respectively. In the initial 202 BV, the N-BC column even brought down phosphate concentration from 1.0 to below 0.01 mg/L, i.e., almost 99% removal rate. On the whole, compared to D201, N-BC exhibited a more excellent treatment ability of phosphate-contaminated wastewater, in accordance with the aforementioned results in Section 3.3. In Figure S6, when introducing NO_3^-, SO_4^{2-}, HCO_3^-, CO_3^{2-}, and HA into influent, the N-BC column yields only ∼50 and 72 BV effluents with breakthrough points of 0.1 and 0.5 mg P/L, respectively, owing to the tremendous interference of these coexisting substances. Moreover, the exhausted N-BC could be effectively regenerated using a wt % NaOH solution of only 10 BV with a desorption rate of more than ∼98%; more importantly, more than 80% desorption was yielded in the initial 3 BV (Figure 6b). To examine the reusability of N-BC, a batch experiment of adsorption−desorption cycles was carried out, and the results are recorded in Figure 6c. It can be discovered that the adsorption capacity of N-BC to phosphate has no perceptible decline after seven adsorption−desorption cycles, and the desorption rate of every cycle was near ∼100%. It suggests that N-BC can achieve repeated use for phosphate removal. It is visible that N-BC is a candidate of great potential for application in decontamination of phosphate-laden wastewater.

3.6. Adsorption Mechanism. As discussed earlier, we speculated the nonspecific out-sphere complexation of the quaternary ammonium groups and phosphate dominated the phosphate retention by N-BC. To further figure out the underlying mechanism, FTIR and XPS analyses of N-BC before and after phosphate loading were performed, and the results are shown in Figure 7. As depicted in Figure 7a, for N-BC, the peaks located at 3440 and 1384 cm^{-1} corresponded to the O−H stretching vibration of the physically bound water and the vibration of the quaternary ammonium groups, respectively. After phosphate loading, a new peak at ∼1048 cm^{-1}, assigned to the stretching vibration of P−O or O−P−O

https://doi.org/10.1021/acsomega.3c10526
ACS Omega 2024, 9, 20119−20128

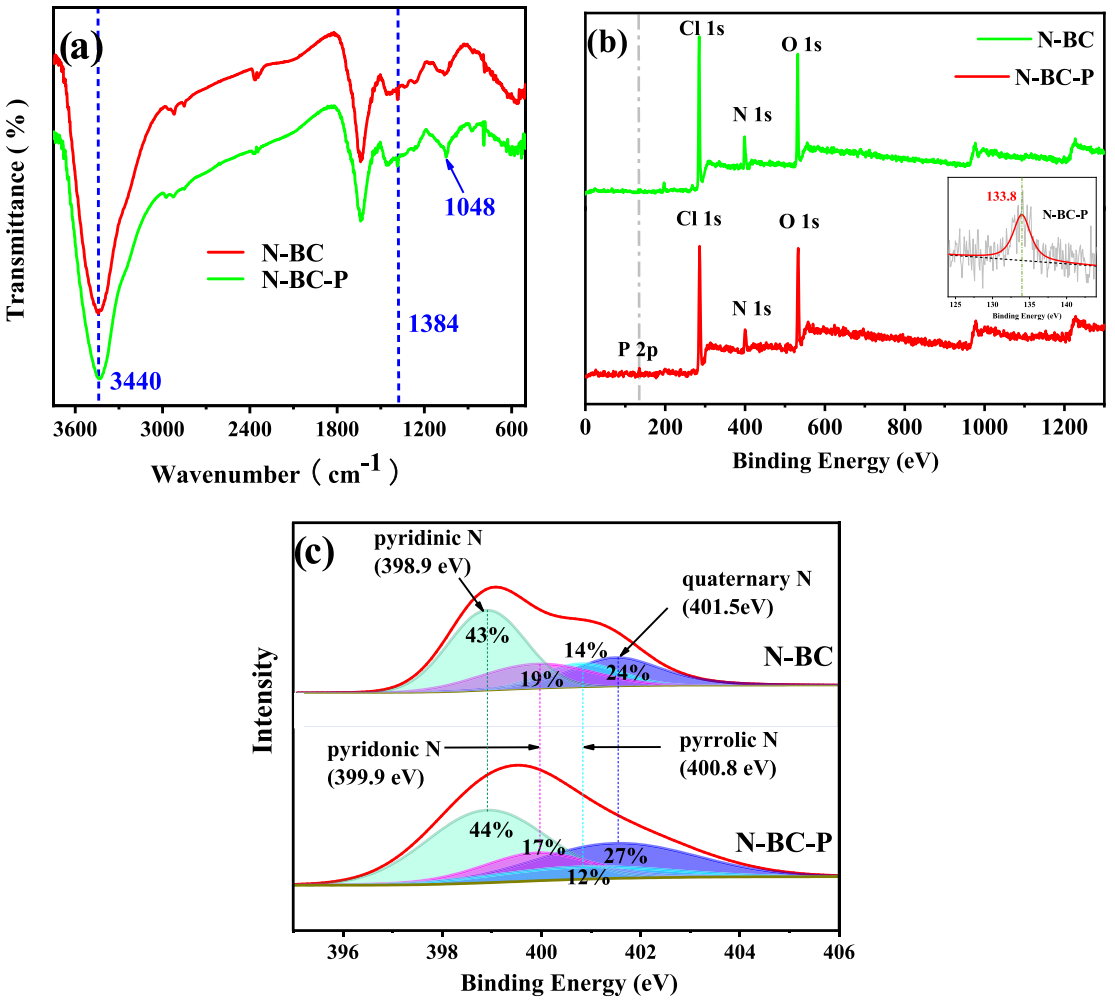

Figure 7. (a) FTIR spectrum of N-BC before and after phosphate adsorption, (b) full XPS spectrum of N-BC before and after phosphate adsorption, and (c) XPS spectrum of N 1s for N-BC with and without phosphate adsorption.

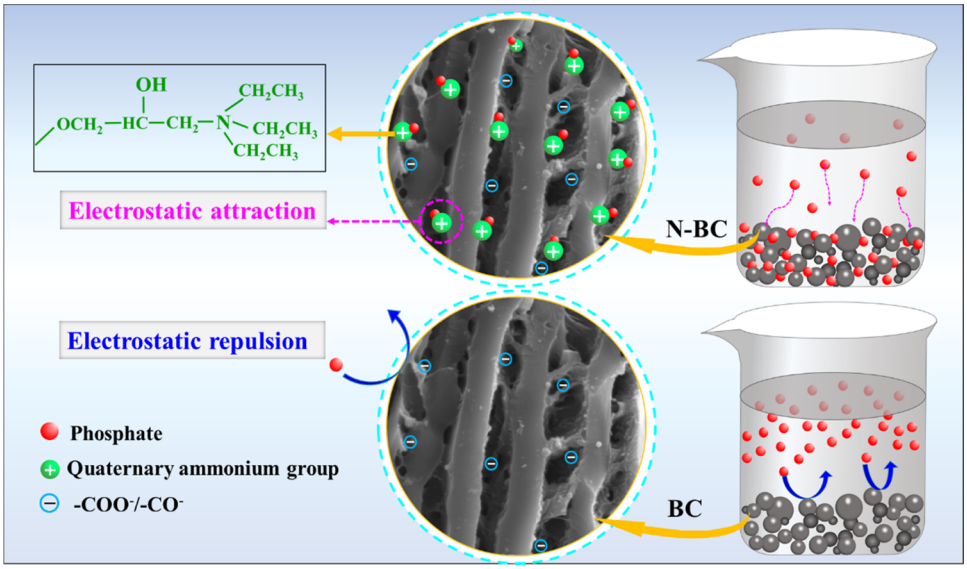

Figure 8. Adsorption mechanism of phosphate onto N-BC.

appeared accompanied by an obvious decline in peak intensity of 1384 cm^{-1}. This clearly implies that the quaternary ammonium groups covalently bound to N-BC played a dominant role in phosphate capture.

https://doi.org/10.1021/acsomega.3c10526
ACS Omega 2024, 9, 20119−20128

Figure 7b shows that after phosphate adsorption, the binding energy of the new P 2p characteristic peak for N-BC located at 133.8 eV, which was identical to that of NaH_2PO_4, suggesting that phosphate was adsorbed through nonspecific affinity, i.e., the electrostatic attraction of the quaternary ammonium groups in N-BC. The high-resolution N 1s spectrum in Figure 7c describes that before phosphate loading, N 1s spectra of N-BC were divided into four main peaks placed at 398.9, 399.9, 400.8, and 401.5 eV, denoting pyridinic N, pyridonic N, pyrrolic N, and quaternary N (eV), respectively.[39] Nevertheless, after phosphate loading, there are no perceptible changes in the position and proportion of the four peaks, also indicating the nature of the nonspecific binding of phosphate onto N-BC. O 1s spectra of N-BC in Figure S7 shows that except for a newborn peak of the P−O group, the position of other O 1s peaks has no change. Based on this discussion, the adsorption mechanism of phosphate onto N-BC is schematically shown in Figure 8.

4. CONCLUSIONS

In summary, a new adsorbent N-BC for highly efficient phosphate removal was exploited by introducing abundant positively charged quaternary ammonium groups into the pristine BC without any phosphate adsorption. The as-prepared N-BC exhibited high adsorption capacity, great speed, and satisfactory anti-interference ability for phosphate sequestration, generally comparable to the widely used phosphate adsorbent D201. Moreover, N-BC was successfully applied in a fixed-bed column for the effective decontamination of phosphate-polluted wastewater. In addition, saturated N-BC could be thoroughly regenerated and reused without any perceptible capacity loss. This study tremendously expanded the application of biochar, which usually serves as an adsorbent for cationic pollutants, to the purification of anionic pollutants such as phosphate.

■ ASSOCIATED CONTENT

Supporting Information

The Supporting Information is available free of charge at https://pubs.acs.org/doi/10.1021/acsomega.3c10526.

Figures of the schematic diagram of the fixed-bed column adsorption facility, compared photograph and FTIR spectrum of the pristine BC and the resultant N-BC, distribution of phosphate species at different solution pH, breakthrough profiles of N-BC and D201 columns, and XPS spectrum of O 1s for N-BC with and without phosphate adsorption; and the table of the comparison of the maximum adsorption capacities of phosphate onto N-BC and other biochar-based adsorbents (PDF)

■ AUTHOR INFORMATION

Corresponding Author

Shunli Wan − *College of Life & Environmental Sciences, Huangshan University, Huangshan 245041, China;* orcid.org/0000-0001-5662-1373; Phone: +86-559-2546552; Email: wsl@hsu.edu.cn

Authors

Yan Li − *College of Life & Environmental Sciences, Huangshan University, Huangshan 245041, China;* orcid.org/0000-0002-1786-4994

Lili Dong − *College of Life & Environmental Sciences, Huangshan University, Huangshan 245041, China*

Xingyu Ren − *College of Life & Environmental Sciences, Huangshan University, Huangshan 245041, China*

Hao Liu − *College of Life & Environmental Sciences, Huangshan University, Huangshan 245041, China*

Chenjia Zhang − *College of Life & Environmental Sciences, Huangshan University, Huangshan 245041, China*

Complete contact information is available at: https://pubs.acs.org/10.1021/acsomega.3c10526

Notes

The authors declare no competing financial interest.

■ ACKNOWLEDGMENTS

The authors greatly appreciate the financial support from the Natural Science Foundation of China (No. 22006047), the Research and Innovation Team Project of Anhui Province (No. 2023AH010053), Talent Fund of Department of Education Anhui Province (Nos. 304021 and gxyq2022085), Fund of the Natural Science Research Project of Universities of Education Department for Anhui Province (Nos. 2023AH051380, KJ2021A1046, and 2022xkjq004), Innovative Training Foundation of College Students of Huangshan University (Nos. 202210375016, 202210375056, and 202210375094), and First-class discipline of Huangshan University (No. ylxk202101).

■ REFERENCES

(1) Gao, Y.; Zhang, W.; Gao, B.; Jia, W.; Miao, A.; Xiao, L.; Yang, L. Highly efficient removal of nitrogen and phosphorus in an electrolysis-integrated horizontal subsurface-flow constructed wetland amended with biochar. *Water Res.* **2018**, *139*, 301−310.

(2) de Rozari, P.; Greenway, M.; El Hanandeh, A. Phosphorus removal from secondary sewage and septage using sand media amended with biochar in constructed wetland mesocosms. *Sci. Total Environ.* **2016**, *569*−*570*, 123−133.

(3) Yang, W.; Shi, X.; Dong, H.; Tang, H.; Chen, W.; Wu, M.; Hua, M.; Zhang, W. Fabrication of a reusable polymer-based cerium hydroxide nanocomposite with high stability for preferable phosphate removal. *Chem. Eng. J.* **2021**, *405*, No. 126649.

(4) Zhang, Y.; Pan, B.; Shan, C.; Gao, X. Enhanced phosphate removal by nanosized hydrated La(III) oxide confined in cross-linked polystyrene networks. *Environ. Sci. Technol.* **2016**, *50* (3), 1447−1454.

(5) Wu, B.; Wan, J.; Zhang, Y.; Pan, B.; Lo, I. M. C. Selective phosphate removal from water and wastewater using sorption: Process fundamentals and removal mechanisms. *Environ. Sci. Technol.* **2020**, *54* (1), 50−66.

(6) Sun, D.; Hong, X.; Wu, K.; Hui, K. S.; Du, Y.; Hui, K. N. Simultaneous removal of ammonia and phosphate by electro-oxidation and electrocoagulation using RuO2−IrO2/Ti and micro-scale zero-valent iron composite electrode. *Water Res.* **2020**, *169*, No. 115239.

(7) Zhang, M.; Lin, K.; Li, X.; Wu, L.; Yu, J.; Cao, S.; Zhang, D.; Xu, L.; Parikh, S. J.; Ok, Y. S. Removal of phosphate from water by paper mill sludge biochar. *Environ. Pollut.* **2022**, *293*, No. 118521.

(8) Gong, L.; Yao, Z.; Zhu, C.; Lian, X.; He, B.; Qu, L.; Xiong, W.; Yu, B. Synthesis of porous Mg(OH)2 nanowires for phosphate removal from water. *Colloid Surf., A* **2023**, *676*, No. 132137.

(9) Venkiteshwaran, K.; Pokhrel, N.; Hussein, F.; Antony, E.; Mayer, B. K. Phosphate removal and recovery using immobilized phosphate binding proteins. *Water Res. X* **2018**, *1*, No. 100003.

(10) Rai, J.; Kumar, D.; Pandey, L. K.; Yadav, A.; Gaur, J. P. Potential of cyanobacterial biofilms in phosphate removal and biomass production. *J. Environ. Manage.* **2016**, *177*, 138−144.

(11) Wan, S.; Wu, J.; He, F.; Zhou, S.; Wang, R.; Gao, B.; Chen, J. Phosphate removal by lead-exhausted bioadsorbents simultaneously achieving lead stabilization. *Chemosphere* **2017**, *168*, 748−755.
(12) Pan, B.; Han, F.; Nie, G.; Wu, B.; He, K.; Lu, L. New Strategy To Enhance Phosphate Removal from Water by Hydrous Manganese Oxide. *Environ. Sci. Technol.* **2014**, *48* (9), 5101−5107.
(13) Mulkerrins, D.; Dobson, A. D. W.; Colleran, E. Parameters affecting biological phosphate removal from wastewaters. *Environ. Int.* **2004**, *30* (2), 249−259.
(14) Chen, D.; Jia, J.; Liao, X.; Zhou, L.; Hu, Z.-T.; Pan, B. Phosphate removal by polystyrene anion exchanger (PsAX)-supporting Fe-loaded nanocomposites: Effects of PsAX functional groups and ferric (hydr)oxide crystallinity. *Chem. Eng. J.* **2020**, *387*, No. 124193.
(15) Zhang, Q.; Zhang, Z.; Teng, J.; Huang, H.; Peng, Q.; Jiao, T.; Hou, L.; Li, B. Highly Efficient Phosphate Sequestration in Aqueous Solutions Using Nanomagnesium Hydroxide Modified Polystyrene Materials. *Ind. Eng. Chem. Res.* **2015**, *54* (11), 2940−2949.
(16) Chiban, M.; Soudani, A.; Sinan, F.; Tahrouch, S.; Persin, M. Characterization and application of dried plants to remove heavy metals, nitrate, and phosphate ions from industrial wastewaters. *Clean-Soil, Air, Water* **2011**, *39* (4), 376−383.
(17) Almanassra, I. W.; Kochkodan, V.; McKay, G.; Atieh, M. A.; Al-Ansari, T. Review of phosphate removal from water by carbonaceous sorbents. *J. Environ. Manage.* **2021**, *287*, No. 112245.
(18) Milovanović, Ž.; Lazarević, S.; Janković-Častvan, I.; Radovanović, Ž.; Cvetković, S.; Janaćković, Đ.; Petrović, R. The removal of phosphate from aqueous solutions by sepiolite/ZrO2 Composites: Adsorption behavior and mechanism. *Water* **2023**, *15* (13), 2376.
(19) Ou, W.; Lan, X.; Guo, J.; Cai, A.; Liu, P.; Liu, N.; Liu, Y.; Lei, Y. Preparation of iron/calcium-modified biochar for phosphate removal from industrial wastewater. *J. Clean. Prod.* **2023**, *383*, No. 135468.
(20) Deng, J.; Xiong, T.; Xu, F.; Li, M.; Han, C.; Gong, Y.; Wang, H.; Wang, Y. Inspired by bread leavening: one-pot synthesis of hierarchically porous carbon for supercapacitors. *Green Chem.* **2015**, *17* (7), 4053−4060.
(21) Xiao, X.; Chen, B.; Chen, Z.; Zhu, L.; Schnoor, J. L. Insight into multiple and multilevel structures of biochars and their potential environmental applications: A critical review. *Environ. Sci. Technol.* **2018**, *52* (9), 5027−5047.
(22) Liu, W. J.; Jiang, H.; Yu, H. Q. Development of biochar-based functional materials: toward a sustainable platform carbon material. *Chem. Rev.* **2015**, *115* (22), 12251−12285.
(23) Meyer, S.; Glaser, B.; Quicker, P. Technical, Economical, and Climate-Related Aspects of Biochar Production Technologies: A Literature Review. *Environ. Sci. Technol.* **2011**, *45* (22), 9473−9483.
(24) Chen, Z.; Xiao, X.; Chen, B.; Zhu, L. Quantification of chemical states, dissociation constants and contents of oxygen-containing groups on the surface of biochars produced at different temperatures. *Environ. Sci. Technol.* **2015**, *49* (1), 309−317.
(25) Keiluweit, M.; Nico, P. S.; Johnson, M. G.; Kleber, M. Dynamic molecular structure of plant biomass-derived black carbon (Biochar). *Environ. Sci. Technol.* **2010**, *44*, 1247−1253.
(26) Li, H.; Dong, X.; da Silva, E. B.; de Oliveira, L. M.; Chen, Y.; Ma, L. Q. Mechanisms of metal sorption by biochars: Biochar characteristics and modifications. *Chemosphere* **2017**, *178*, 466−478.
(27) Vikrant, K.; Kim, K. H.; Ok, Y. S.; Tsang, D. C. W.; Tsang, Y. F.; Giri, B. S.; Singh, R. S. Engineered/designer biochar for the removal of phosphate in water and wastewater. *Sci. Total Environ.* **2018**, *616*−*617*, 1242−1260.
(28) Jung, K. W.; Hwang, M. J.; Ahn, K. H.; Ok, Y. S. Kinetic study on phosphate removal from aqueous solution by biochar derived from peanut shell as renewable adsorptive media. *Int. J. Environ. Sci. Technol.* **2015**, *12* (10), 3363−3372.
(29) Almanassra, I. W.; McKay, G.; Kochkodan, V.; Ali Atieh, M.; Al-Ansari, T. A state of the art review on phosphate removal from water by biochars. *Chem. Eng. J.* **2021**, *409*, No. 128211.
(30) Wang, W.-Y.; Yue, Q.-Y.; Xu, X.; Gao, B.-Y.; Zhang, J.; Li, Q.; Xu, J.-T. Optimized conditions in preparation of giant reed quaternary amino anion exchanger for phosphate removal. *Chem. Eng. J.* **2010**, *157* (1), 161−167.
(31) Xu, X.; Gao, B.; Wang, W.; Yue, Q.; Wang, Y.; Ni, S. Adsorption of phosphate from aqueous solutions onto modified wheat residue: Characteristics, kinetic and column studies. *Colloids Surf., B* **2009**, *70* (1), 46−52.
(32) Hu, Y.; Du, Y.; Nie, G.; Zhu, T.; Ding, Z.; Wang, H.; Zhang, L.; Xu, Y. Selective and efficient sequestration of phosphate from waters using reusable nano-Zr(IV) oxide impregnated agricultural residue anion exchanger. *Sci. Total Environ.* **2020**, *700*, No. 134999.
(33) Shang, Y.; Xu, X.; Qi, S.; Zhao, Y.; Ren, Z.; Gao, B. Preferable uptake of phosphate by hydrous zirconium oxide nanoparticles embedded in quaternary-ammonium Chinese reed. *J. Colloid Interface Sci.* **2017**, *496*, 118−129.
(34) Xu, X.; Gao, B.; Yue, Q.; Zhong, Q. Sorption of phosphate onto giant reed based adsorbent: FTIR, Raman spectrum analysis and dynamic sorption/desorption properties in filter bed. *Bioresour. Technol.* **2011**, *102* (9), 5278−5282.
(35) Ho, Y.-S. Second-order kinetic model for the sorption of cadmium onto tree fern: A comparison of linear and non-linear methods. *Water Res.* **2006**, *40* (1), 119−125.
(36) Huang, Y.; Lee, X.; Grattieri, M.; Yuan, M.; Cai, R.; Macazo, F. C.; Minteer, S. D. Modified biochar for phosphate adsorption in environmentally relevant conditions. *Chem. Eng. J.* **2020**, *380*, 122375 DOI: 10.1016/j.cej.2019.122375.
(37) Allen, S. J.; McKay, G.; Khader, K. Y. H. lntraparticle diffusion of a basic dye during adsorption onto sphagnum peat. *Environ. Pollut.* **1989**, *56*, 39−50.
(38) Wan, S.; Qiu, L.; Tang, G.; Chen, W.; Li, Y.; Gao, B.; Hea, F. Ultrafast sequestration of cadmium and lead from water by manganese oxide supported on a macro-mesoporous biochar. *Chem. Eng. J.* **2020**, *387*, No. 124095.
(39) Ling, L. L.; Liu, W. J.; Zhang, S.; Jiang, H. Magnesium Oxide Embedded Nitrogen Self-Doped Biochar Composites: Fast and High-Efficiency Adsorption of Heavy Metals in an Aqueous Solution. *Environ. Sci. Technol.* **2017**, *51* (17), 10081−10089.

https://doi.org/10.1021/acsomega.3c10526
ACS Omega 2024, 9, 20119−20128